

Chapter 6

Electrochemical Aspects of Chemical Mechanical Polishing

K. Cadien, L. Nolan, H. Pirayesh, K. Dawkins, and Z. Xu

6.1 Introduction

Metal and glass surfaces have been polished to high levels of planarity and tight tolerances for hundreds of years. The telescope of Galileo, for instance, was enabled by accurate glass lens polishing. Chemical Mechanical Polishing, also known as chemical mechanical planarization or CMP, was developed specifically for the semiconductor industry from the same historical principles, beginning in 1983 at IBM [1] with the successful planarization of reflowed glass “bulges” on a wafer surface. Although reflowed glass was never adopted as a commercial technique, and despite initial reluctance to incorporate the use of small particles into cleanroom technology, the use of CMP has flourished. Today, a typical integrated circuit is polished dozens of times during manufacture; the planarization of each device layer permits new layers to be built upon it, leading to devices with eight or more separate layers of metallization. CMP is thus industrially important as an enabler of new geometries, as well as a manufacturing technique in its own right.

CMP technology has evolved considerably since its inception and is now well established for metals such as tungsten, aluminum, and copper. Techniques for polishing semiconductors such as single crystal and polycrystalline silicon were also developed. Dielectric materials such as silicon dioxide and tantalum nitride have also been thoroughly investigated. Future challenges for CMP have been

K. Cadien (✉) • H. Pirayesh • K. Dawkins • Z. Xu
Department of Chemical and Materials Engineering, University of Alberta,
9107 – 116 Street, Edmonton, AB, Canada T6G 2 V4
e-mail: kcadien@ualberta.ca

L. Nolan
Portland Technology Development, Intel Corporation, Hillsboro, OR, USA

identified in the International Technology Roadmap for Semiconductors and they include [2]:

- Increasing within-wafer removal rate uniformity and decreasing dishing for shallow-trench isolation (STI)
- Reducing scratching and other defects
- Scaling to 450 mm wafers

CMP should not be confused with ECMP, or Electrochemical Mechanical Polishing, a separate but related polishing technique in which a voltage is applied to a conducting surface during polishing, making it the working electrode in a three-electrode electrochemical cell. In ECMP, polishing is achieved by electrochemical dissolution of the working electrode rather than by mechanical means. This allows low polishing pressures and very low abrasive particle concentrations to be used, but does not typically achieve the same surface planarity as CMP [3]. This technique is not discussed here.

6.1.1 CMP Tools

The typical CMP tool consists of a carrier which supports the wafer and presses it down against the polishing pad, while both the pad and carrier (and hence wafer) rotate. A polishing slurry, containing water, chemical components, and fine abrasives, is introduced onto the polishing pad so that it flows between the pad and wafer. The pad is usually significantly larger than the wafer and is mounted on a platen that resists the load from the wafer. Polishing pads are polymeric and may have grooves inscribed on the surface to assist in slurry distribution. They may also contain microscopic pores, creating asperities, or peaks, on the pad surface. The asperities gradually wear away with use and the pad becomes “glazed,” resulting in a drop in polishing rate; to counteract this, a diamond-grit disc conditioner passes across the pad during polishing to maintain a consistent surface. Schematic representations of these components are shown in Figs. 6.1 and 6.2.

Basic CMP tools used for research have been assembled from these components by using, for example, a modified drill press as the wafer carrier and a metallurgical polishing wheel as the platen. More sophisticated research-grade CMP tools have these components preassembled and may additionally contain vacuum chucks to grip the wafer, and some robotic parts to automate wafer loading and unloading. Specialist metrology instruments may also be installed to monitor friction, pad temperature, acoustic emissions, and other process parameters. Industrial CMP tools are self-contained “dry-in, dry-out” units which process cassettes of wafers on multiple platens and incorporate wafer cleaning and drying. These typically also contain dedicated metrology instruments. Regardless of tool type, the user controls the process by selecting the polishing pad and slurry, the rate at which slurry flows on to the pad, the speed of wafer and platen rotation, and the pressure applied to the system.

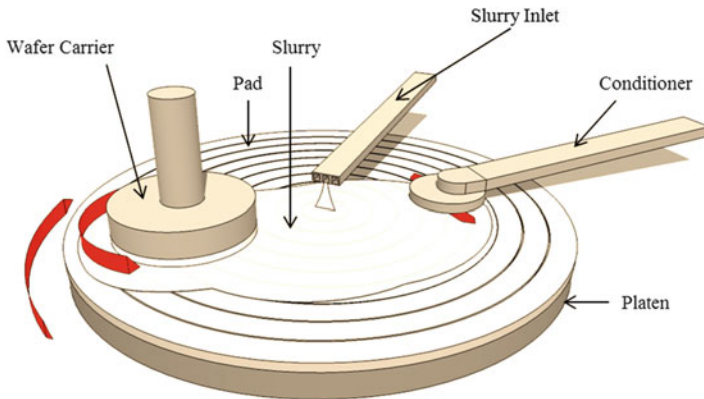
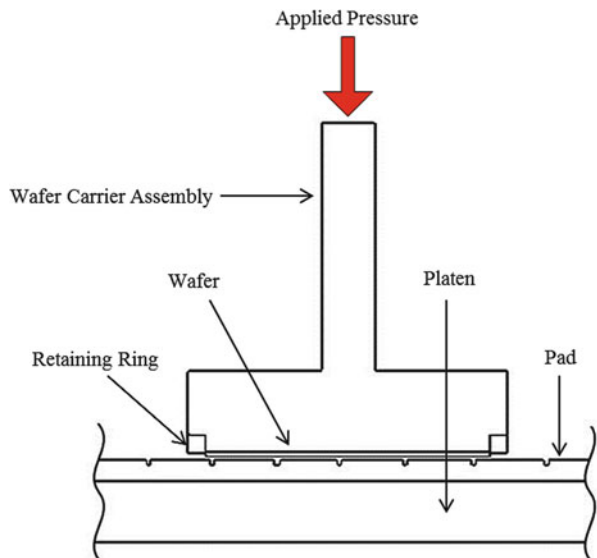


Fig. 6.1 Schematic diagram showing the typical polishing components

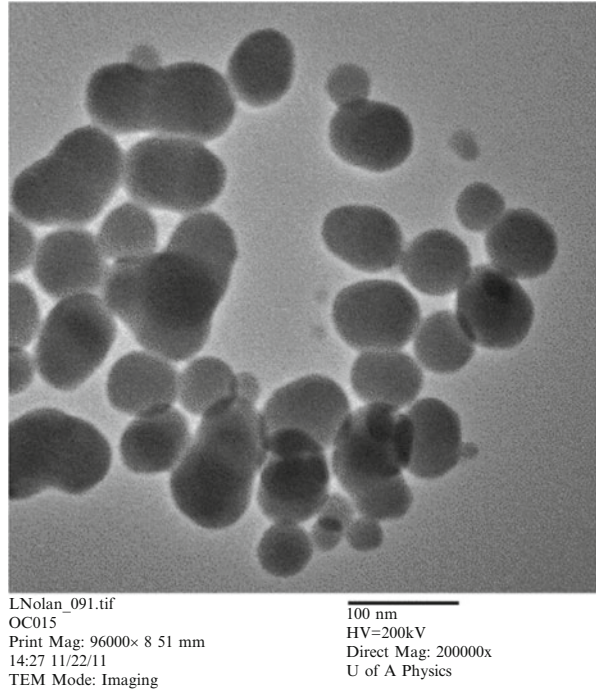
Fig. 6.2 Cross section through wafer carrier, showing position of wafer



Unlike many other nanofabrication techniques, CMP is carried out in ambient conditions and does not require special conditions beyond a clean environment to prevent unwanted particulates from contaminating the process.

The polishing slurry, polishing pad, and conditioning disk are consumed during processing and must be periodically replaced. These components determine polishing outcomes and make up a significant portion of the tools' cost of ownership, so they should be selected carefully. The typical features and components of these consumables are described below.

Fig. 6.3 TEM micrograph of colloidal silica abrasives (bright field image, direct magnification = $\times 200,000$)



6.1.2 Slurry

CMP slurries are aqueous and contain components to bring about both chemical and mechanical effects on the wafer. Mechanical work is brought about by abrasive particles of between 20 nm and several microns in size. These are typically hard oxides such as silica, alumina, and ceria, although softer polymeric abrasives have been investigated in order to reduce defects [4]. Mixtures of different types of oxides have also been used in order to exploit the properties of multiple abrasive types, such as the high removal rates associated with ceria and the low cost and good size control of silica [5, 6]. Small abrasives are generally fabricated through a colloidal process and hence are approximately spherical in shape. Larger abrasives may be crushed and are jagged. Specialty abrasive shapes, such as cubes, prolate spheroids, and flakes, have also been used experimentally. A TEM image of colloidal silica particles is shown in Fig. 6.3, while mixed-oxide particles of unconventional shape are shown in Fig. 6.4.

Increasing polishing rates with decreasing particle size have been demonstrated when polishing tungsten with alumina particles, down to a particle size of 250 nm [7]. Some dependence of polishing rate on particle size distribution has also been observed [8]. However, a clear decrease in polish rate is observed with very small particles, suggesting that the abrasives must be larger than a critical size to be effective [5]. An example of this is the work of Lin et al. [5]. The study

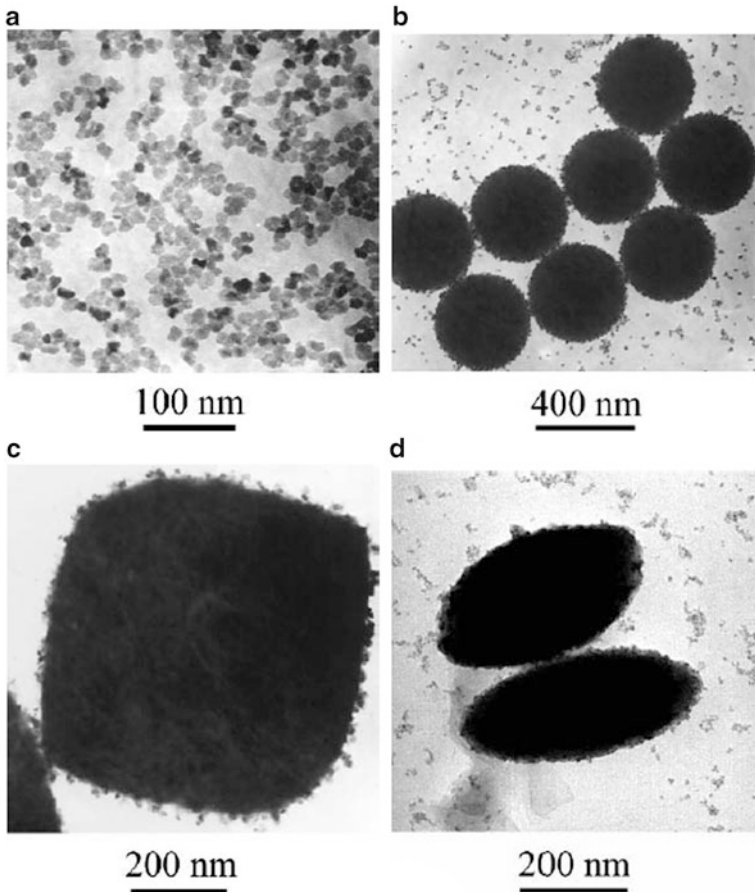


Fig. 6.4 TEM micrographs of (a) ceria particles, mean diameter of 20 nm; (b) 400 nm colloidal silica particles mixed with the ceria particles shown in (a)—electrostatic attraction ensures adhesion of ceria to silica; (c) 700 nm cubic hematite coated in 35 nm of silica, mixed with the ceria particles shown in (a); 400 nm ellipsoidal hematite coated in 35 nm of silica, mixed with the ceria particles shown in (a) (Reproduced from [6])

demonstrated a 20-fold increase in oxide polish rates when using composite particles of a silica to ceria weight ratio of 0.1 (5 wt% silica particles and 0.5 wt% ceria particles), compared to polishing with either silica or ceria alone. This is due to the fact that ceria particles are very small and acting alone as polishing slurry cannot effectively transfer the shear forces from the pad to the wafer.

The concentration of particles in the slurry also affects the rate of polishing. Numerous studies have indicated an increase in polishing rate with increasing abrasive concentration, up to a critical concentration [7, 9]. If the amount of abrasives is increased beyond this point, no further increase in polishing rate is

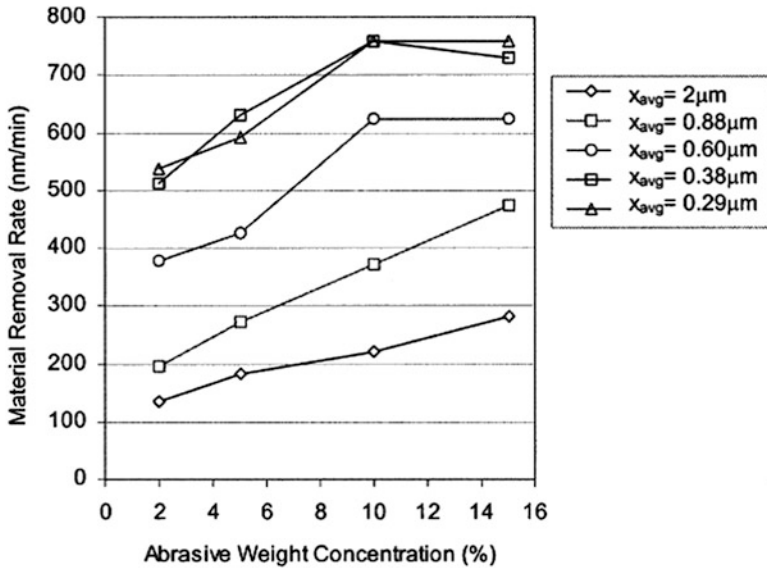


Fig. 6.5 Removal rate of Tungsten by silica particles of the sizes indicated increases with increasing abrasive concentration, until a constant rate is reached. Further increases in abrasive concentration do not result in any further polish rate increases (Reproduced from [8])

observed, and in fact the polishing rate may decrease. This has been observed in both tungsten and copper CMP, using abrasives ranging from around 85 nm to 2 μm in diameter, as illustrated in Figs. 6.5 and 6.6.

Chemical work during polishing is brought about by the addition of oxidizers, corrosion inhibitors, chelating agents, pH adjusters, buffers, and surfactants. These vary considerably, depending on the surface to be polished, and will be discussed in the appropriate part of Sect. 6.3. It should be noted that the active components make up only a small fraction (typically 10 wt% or less) of the slurry, with water making up the remainder.

6.1.3 Pads and Conditioners

Polishing pads are polymeric and relatively soft, with a durometer hardness between 55 Shore A and 60 Shore D, depending on their application [10]. They are often made of a polyurethane blend and contain microscopic pores. A cross-sectional SEM image of a typical pad is shown in Fig. 6.7. The surface of the pad is swept by a diamond-grit conditioner during polishing. This continually refreshes the surface and opens pores, resulting an approximately constant microscopic surface roughness. The sizes of asperities on the pad have, like many rough surfaces, been shown to follow an approximately Gaussian distribution [11, 12].

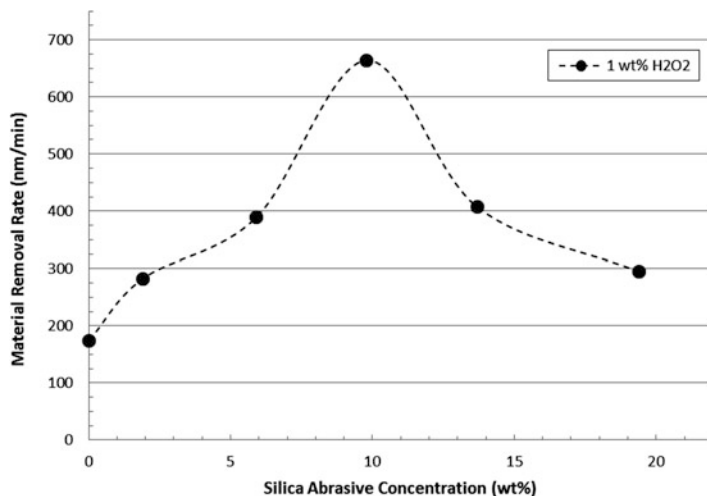


Fig. 6.6 Removal rate of Copper by silica particles with mean diameter of 84 nm indicates that removal rate increases with increasing abrasive concentration, up to a maximum value. Further increases in abrasive concentration decrease the polishing rate (Plotted from data in [9])

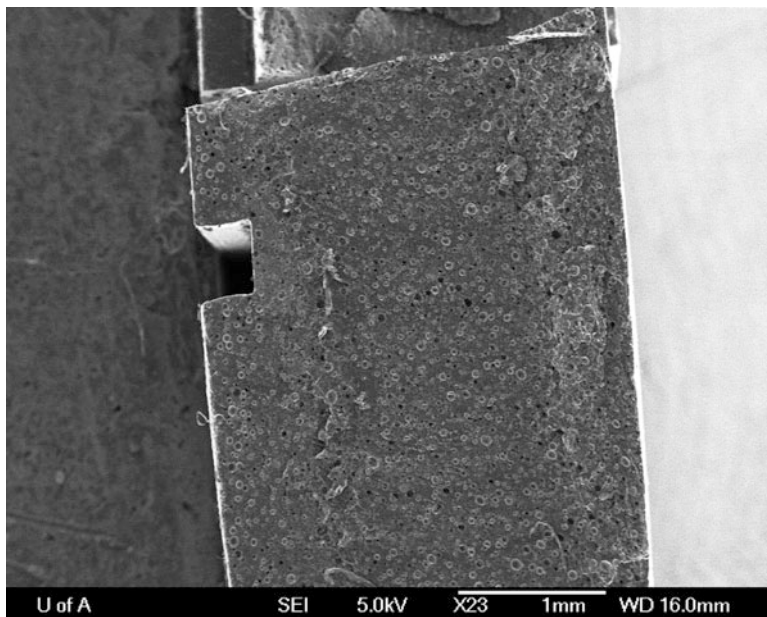


Fig. 6.7 Cross-sectional SEM of a typical polishing pad. Numerous pores and the cross section of a groove are visible

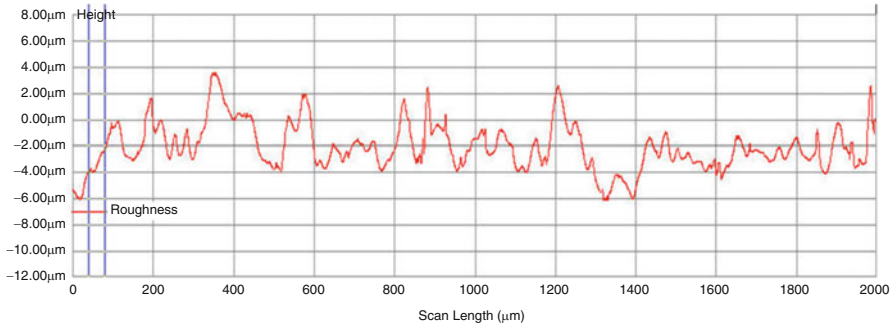


Fig. 6.8 Profilometer scan of pad surface (Scan length 2 mm, total y-axis height 20 μm)

A profilometry scan of the surface is shown in Fig. 6.8. Typical values for the average pad roughness are between 1 and 20 μm .

Polishing pads are often grooved to facilitate slurry transport across the surface. This is important as the slurry must travel from near the center of the pad to a radial distance equal to the outer edge of the wafer, a length of 30 cm or more, under the centrifugal action of the rotating pad alone. Common pad groove patterns include spirals, radial and/or concentric lines, square grids, and logarithmical or “k” grooves. Despite such patterning, utilization of slurry in the CMP process is thought to be fairly low, with published estimates ranging from 90 % to as low as 2 %, depending on process conditions [13, 14]. Given that slurry costs make up a significant portion of CMP cost of ownership and that treating slurry waste after polishing is a significant burden on fabrication facilities, increasing slurry utilization is an important driver in CMP research.

6.1.4 Pressure and Velocity: The Preston Equation

Aside from the choice of consumables, the two main parameters controlled by the user are the rotational speed of the wafer and pad and the pressure or “downforce” exerted on the wafer. The relationship between pressure, velocity, and the overall rate of material removal has therefore been the subject of considerable research. One of the earliest and most widely known of these relationships is the Preston equation, which was developed in 1927 to describe plate glass polishing [15]. Equation (6.1) states that the removal rate (MRR) is proportional to the product of the velocity (V) and applied pressure (P). The proportionality constant K_P is known as the Preston coefficient and is experimentally determined for a given system.

$$\text{MRR} = K_p \times PV \quad (6.1)$$

The term “system” in this context refers to a tool type and its consumables, such as the surface being polished, the polishing pad and slurry, and the conditioner type and regime. This highlights the limitation of the Preston equation: while useful within a system, the data obtained from one tool or set of consumables cannot be transferred to another. Additionally, some experimental work is required to determine the value of the constant before the relationship can be used.

A number of models which attempt to overcome these limitations have been developed in response to industry calls for a priori design capabilities. These are based on various understandings of the mechanisms at work during CMP, such as the rates of chemical interactions [16, 17] or the force between the abrasives and the wafer [18–20], and incorporate techniques such as fluid dynamics and finite element analysis [21–23]. Many also require some experimentally derived quantities as model inputs. Pressure and velocity are usually incorporated by assessing their impact on the frequency of the modeled polishing event. The output of the model, typically the overall polish rate, is obtained by summing these events over a specified time interval.

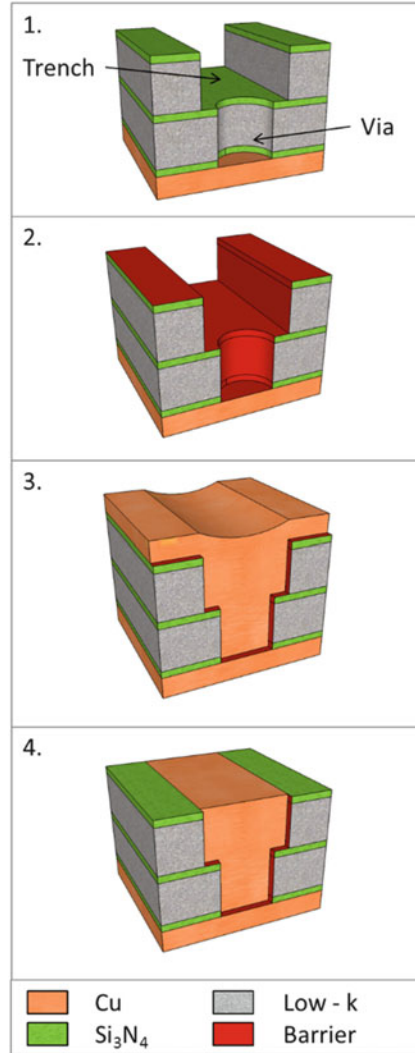
The models referenced here are just some of a plethora of such models, and the interested reader is directed to the CMP literature for a more complete list. The lack of wide acceptance for any one of these models over the others reflects the ambiguity surrounding the fundamental polishing actions, and the difficulty of directly characterizing the CMP process. However, good progress has been made in in situ measurement techniques, and models are becoming more accurate and more widely used.

6.2 CMP Fabrication Techniques

There are many fabrication techniques in which CMP plays a crucial role, and two of the most widely used are STI and copper dual damascene.

The dual damascene method is used to fabricate copper-filled vias and trenches to connect chip components. In this method, the vias and trenches are etched through multiple layers of low-k dielectric and silicon nitride capping material. The internal surface of the etched parts is then coated in a very thin layer of a barrier material, such as tantalum, to prevent diffusion of copper from the interconnect into the device and to act as a seed for electrochemical deposition of the fill metal. Copper is then deposited into the vias and trenches; however, in order to fill the trench completely, and an excess is deposited in non-patterned areas. CMP is then done afterward to remove the excess copper and the diffusion barrier from the surface of the chip, leaving a flush connecting structure. The process is shown schematically in Fig. 6.9. This technique can be performed by etching either the

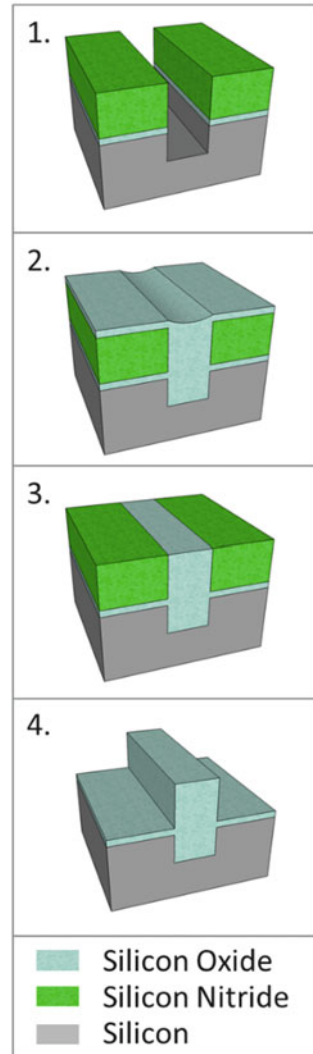
Fig. 6.9 Schematic of the dual damascene process: Trenches and vias are etched through device layers (1) and then a diffusion barrier is deposited (2). An excess of copper is deposited to ensure that the interconnect structure is completely filled (3). The excess copper and the diffusion barrier are then removed using CMP (4), leaving a planar surface



trench first (“trench-first dual damascene”) or the via first (“via-first dual damascene”). Where only one structure is created, filled, and polished at a time, the technique is referred to simply as “damascene.”

The STI method is used to electrically isolate transistors embedded in the silicon substrate from one another and is also enabled by CMP. In this technique, illustrated in Fig. 6.10, a trench is cut into the silicon substrate using a hard silicon nitride layer as mask. The trench is then overfilled with CVD silicon oxide to ensure complete filling. CMP is used to remove excess oxide and to planarize the top of the filled trench. The nitride mask is then stripped away, leaving an isolating structure behind.

Fig. 6.10 Schematic of the STI process: a trench is cut through the silicon nitride cap layer into the silicon substrate (1) and excess silicon oxide is deposited (2). CMP is then used to planarize the surface, removing the excess oxide (3). Finally, the nitride cap is removed (4), leaving a trench structure in the silicon that isolates one region from the next



6.3 Electrochemical Phenomena in CMP

In the previous section, CMP techniques used for both conducting and dielectric materials were described. While there are many practical similarities between polishing the two material types, the underlying mechanisms for polishing conductors such as metals are based on electrochemical principles. The principles of the polishing of dielectrics are non-electrochemical by nature and as such will not be discussed further. The remainder of this chapter therefore focuses on the polishing of metals and other conducting materials.

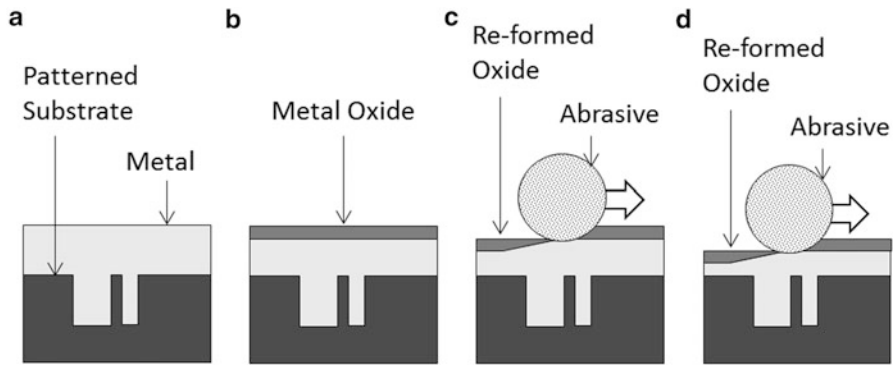


Fig. 6.11 Schematic of the metals CMP mechanism: the patterned metal surface (a) is oxidized by the chemical components of the slurry (b). The oxide layer is then removed by abrasion (c). This process is repeated (d) until the metal is removed and the metal-filled patterns remain

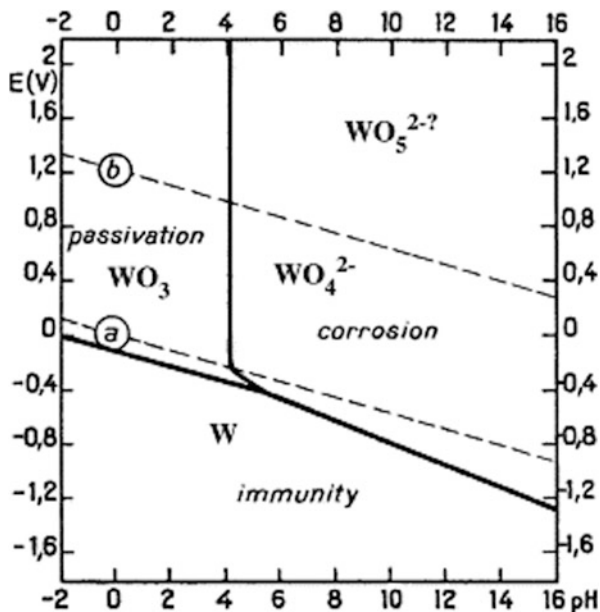
6.3.1 Tungsten CMP

Chemical mechanical polish was developed initially to process vitreous materials. The first metal CMP process was introduced some 15 years later as a more reliable and reproducible alternative to plasma etching for the formation of tungsten plugs at the sub-0.35 μm node [24]. Rather than the “chemical tooth” identified as the primary removal mechanism in oxide polishing [25], W-CMP relies on the sequential oxidation and then removal of the metal surface. This is shown schematically in Fig. 6.11. Due to their ductility, metals are typically difficult to remove without causing damage to the surface. By forming a hydrated oxide as the abradable layer, the hardness and ductility of the polishing surface are reduced, while the metal underneath is protected from ongoing, uncontrolled etching. Both an oxidizer and an abrasive are required for polishing to occur [9].

The key chemical requirements of the metal CMP slurry include both oxidation and passivation of the surface. An initial design point for such a slurry is the potential pH, or Pourbaix, diagram, which is calculated from thermodynamic data and shows the equilibrium relationship between pH, potential, and oxidation products formed. The Pourbaix diagram for tungsten in water is shown in Fig. 6.12. From this figure, it is apparent that passivation of tungsten occurs at all positive potentials at a pH of 4 or lower. Consequently, polishing slurries for tungsten contain an oxidizer, such as hydrogen peroxide, nitric acid, or ferric nitrate, and have a pH of less than 4.

Characterization of the electrochemical behavior of tungsten can be a useful tool in assessing new slurry chemistries. For example, Lim et al. [27] have used techniques such as cyclic voltammetry and potentiodynamic polarization to characterize the formation of tungsten oxidation products. They demonstrated that a continuous, passivating oxide can be induced on the metal surface of tungsten and that the formation of such an oxide leads to improved CMP outcomes.

Fig. 6.12 Pourbaix diagram for tungsten in water [26]

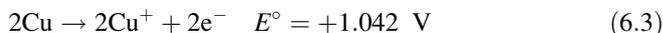
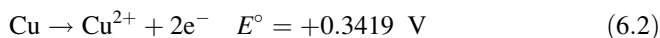


6.3.2 Copper CMP

The process of polishing copper is somewhat more complicated than polishing tungsten or other self-passivating metals such as aluminum. Unlike these metals, copper does not form a stable oxide layer by itself and uncontrolled oxidation can lead to pitting and etching of the copper surface. To counter this, the chemical components of the polishing slurry are manipulated to produce controlled electrochemical effects by including both an oxidizer to form a reacted oxide surface layer and a corrosion inhibitor to stabilize the oxide layer and prevent unwanted, excessive corrosion. Each of these components has a specific electrochemical function which will be discussed in the following sections.

6.3.2.1 Oxidizers

In the presence of water at standard conditions, neither Cu(I) nor Cu(II) oxides form spontaneously. This is confirmed by the negative standard potentials for the formation of CuO and Cu₂O:



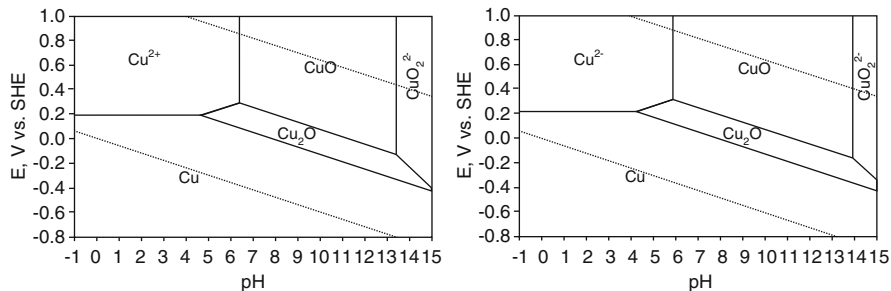


Fig. 6.13 Pourbaix diagrams for the copper–water system at 25 °C. The diagram on the left is for a total dissolved copper activity of 10^{-5} , while the one on the right is for $a_{\text{CuT}} = 10^{-4}$ [29]



To induce oxidation of copper, an oxidizer is added to the slurry. Commonly used oxidizers are nitric acid (HNO_3), ammonium hydroxide (NH_4OH), and hydrogen peroxide (H_2O_2). These are discussed individually below.

Nitric Acid

Nitric acid was one of the first oxidizers selected for copper CMP because nitrate ions promote the formation of Cu(II) ions, rather than Cu(I) ions, and hence CuO rather than Cu_2O , which has been associated with more robust polishing [28]. However, the high pH of strong acids such as nitric acid encourages the dissolution of copper, as indicated by the Pourbaix diagram in Fig. 6.13. Potentiodynamic scans of copper in nitric acid, such as that shown in Fig. 6.14, show that this dissolution is more prominent than oxidation, and nitric acid does not effectively passivate the copper surface. While removal rates for nitric acid are fast, the etching action also results in poor final planarization. In one study, Carpio et al. [30] demonstrated that polishing with nitric acid actually increased the roughness of the copper surface by a factor of 15, with the surface roughness increasing from 10 to 150 Å after polishing.

Ammonium Hydroxide

Ammonium hydroxide has also been examined as an oxidizer in copper CMP because of its ability to passivate copper in potentiodynamic studies. An example of such a study is shown in Fig. 6.15.

This effect is thought to be at least partially due to the production of hydroxide ions by NH_4OH in solution, raising the pH to the point where oxide formation is thermodynamically favorable according to the Pourbaix diagram in Fig. 6.13.

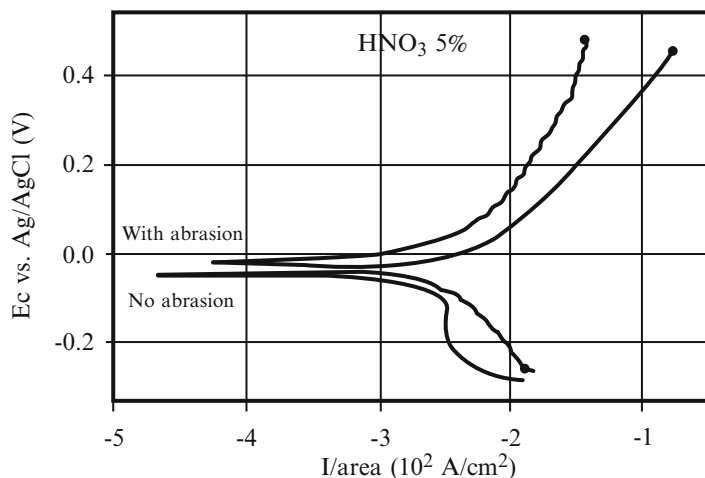


Fig. 6.14 Potentiodynamic profiles for copper in a solution of 5% HNO_3 in air-saturated water, with and without abrasion during testing. The scan rate was 5 mV/s, starting at 0.25 V below the open circuit potential [28]

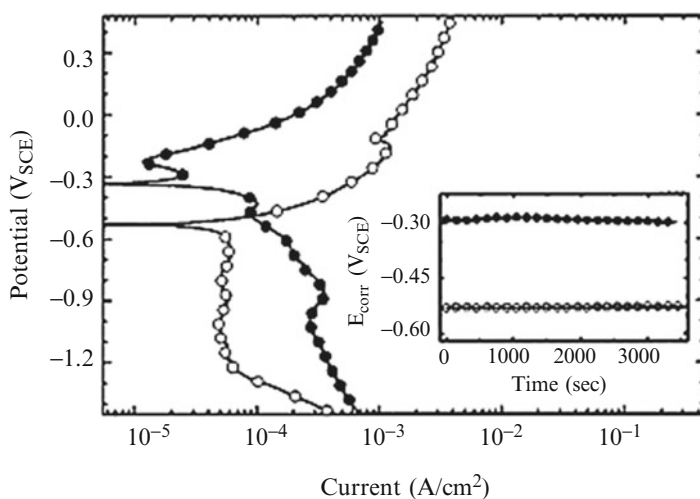
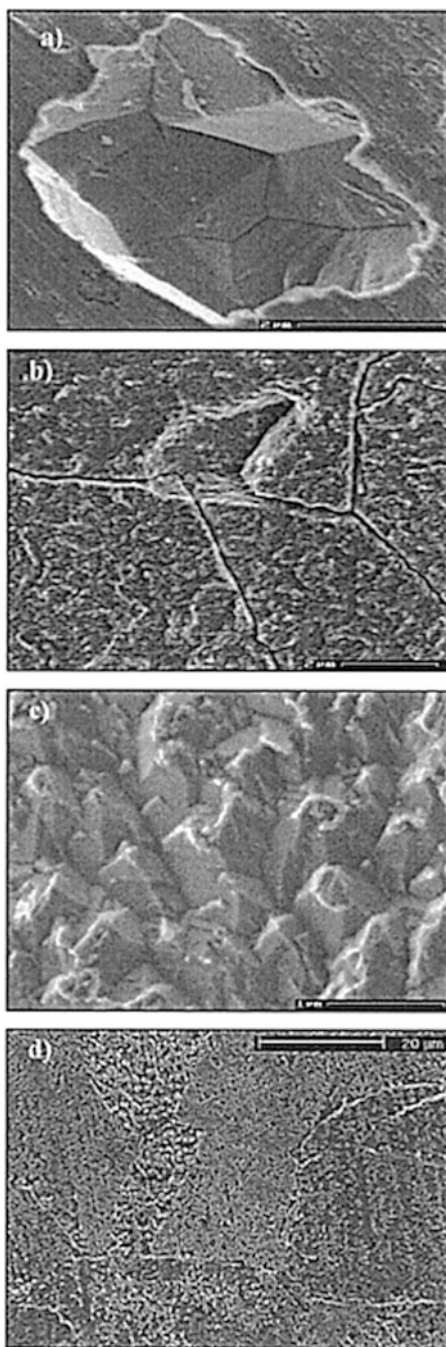


Fig. 6.15 Potentiodynamic profiles of copper in solutions with low (2.35 g/L, filled circle) and high (30 g/L, open circle) concentrations of ammonium hydroxide. Here the scan rate was 1 mV/s. Prior to the commencement of testing, the system was allowed to reach steady state for an hour. The recorded open circuit potential E_{corr} over this hour is shown in the inset [31]

However, ammonia ions also chelate the cupric oxide formed on the copper surface, encouraging dissolution. The overall effect on the passive film is that it is weakened, and pronounced intergranular corrosion may occur. Examples of this type of uncontrolled corrosion are shown in Fig. 6.16 in scanning electron micrographs of copper surfaces polished in different concentrations of ammonium hydroxide for

Fig. 6.16 SEM images of copper surfaces exposed to varying concentrations of NH_4OH at the open circuit potential for varying lengths of time: weak solution (2.35 g/L) for (a) 1 min and (b) 1 h, and strong solution (30 g/L) for (c) 1 min and (d) 1 h [29]



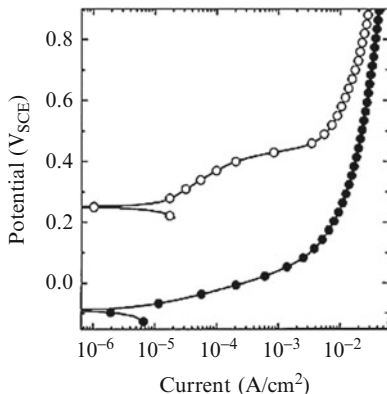


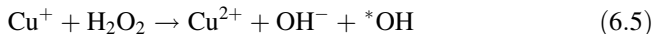
Fig. 6.17 Potentiodynamic profiles for copper electrodes without H_2O_2 (filled circle) and with 3 vol.% H_2O_2 (open circle). The solution is buffered at pH 4 and also contains 10 g/L Na_2SO_4 to increase the solution conductivity. The scan rate is 5 mV/s and the increase in E_{corr} observed is approximately 0.35 V [32]

varying lengths of time. The copper corrosion occurs primarily between the grains and in some cases is severe enough to excise an entire grain, as demonstrated in Fig. 6.16a.

Ammonium hydroxide also has relatively slow corrosion rates, with studies indicating that i_{corr} for copper in a 5 % solution of NH_4OH is just 0.3304 mA/cm^2 , more than 30 times less than i_{corr} for copper in a 5 % solution of nitric acid [31]. Although the chemical reaction rate does not correlate linearly with the overall material removal rate [9], slow corrosion rates in potentiodynamic studies can indicate that the studied oxidizer is not appropriate.

Hydrogen Peroxide

Hydrogen peroxide has become the oxidizer of choice for copper CMP, both as pure H_2O_2 or when present in polishing slurry as a dissolution product of chemicals such as sodium percarbonate. Hydrogen peroxide is a strong oxidizer in and of itself, and can additionally decompose into hydroxyl radicals. This decomposition is catalyzed by transition metal ions, such as Cu^{2+} , which are thought to be abundant in copper CMP slurries during processing. This process is known as the Fenton cycle and occurs by the following reactions:



Hydrogen peroxide in copper polishing slurries therefore leads to a sharp increase in oxidation potential E_{corr} , as demonstrated in the potentiodynamic curves shown in Fig. 6.17. However, strong oxidation is not the only criterion in

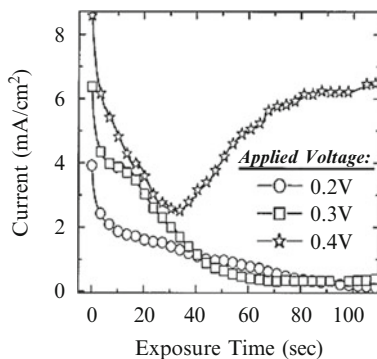


Fig. 6.18 Chronoamperometric profiles of copper in a solution of 3 vol.% H_2O_2 with 10 g/L of Na_2SO_4 , buffered at pH 4. Measurements are taken at potentials of 0.2, 0.3, and 0.4 V. The current stabilizes at a low value for potentials at or below 0.3 V, indicating the development of an oxide film on the copper surface [30]

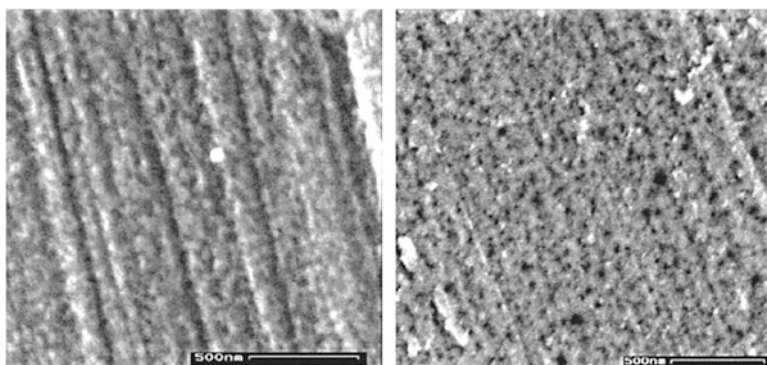


Fig. 6.19 HRSEM of copper exposed to a solution of 3 vol.% H_2O_2 with 10 g/L of Na_2SO_4 , buffered at pH 4 for 5 min at a potential of 0.3 V (*left*) and 0.4 V (*right*). The image on the *left* shows a tightly formed oxide layer, while that on the *right* contains numerous pits (visible as *small black dots*). These results are consistent with the chronoamperometric study performed by the same authors and shown in Fig. 6.18 [30]

determining whether a chemical is appropriate for use as a CMP oxidizer or not. In contrast to ammonium hydroxide, chronoamperometric studies of copper in hydrogen peroxide solutions, such as the one shown in Fig. 6.18, demonstrate that this oxidizer can develop an oxide film without severe intergranular corrosion. High-resolution scanning electron micrographs (HRSEM) are used to confirm the quality of the surface film, as shown in Fig. 6.19. In this figure, the passive film is adherent and continuous at an applied potential of 0.3 V, in good agreement with the chronoamperometric profile shown in Fig. 6.18.

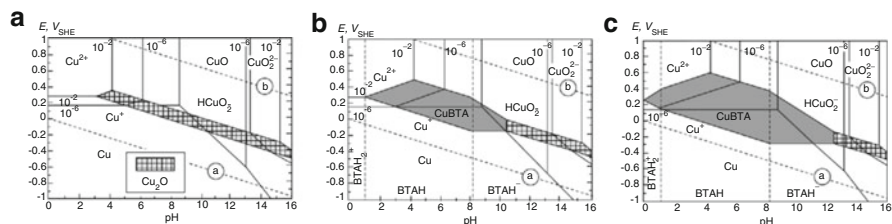


Fig. 6.20 Pourbaix diagrams for (a) copper in water, (b) copper in water with a total activity of BTAH of 10^{-4} , and (c) copper in water with a total activity of BTAH of 10^{-2} . (Originally published in [34], reproduced here from redrawn figure in [35])

Similarly, the breakdown of the film indicated by the chronoamperometric profiles in Fig. 6.18 at an applied voltage of 0.4 V corresponds with the presence of pits at the same voltage in Fig. 6.19. In this example, chronoamperometric characterization can confirm that passivation occurs quickly and that the resulting oxide film is passivating, two essential requirements for use in CMP. The stability of the film formed can be enhanced further when corrosion inhibitors are used in conjunction with oxidizers such as hydrogen peroxide. These are discussed in the next section.

6.3.3 Corrosion Inhibitors

Corrosion inhibitors increase the stability of the passive film initiated by oxidation through adsorption on the oxide surface. Benzotriazole (BTAH) is one of the most commonly used corrosion inhibitors for copper and has been used as a corrosion inhibitor in cooling water systems for close to 50 years [33]. Alternative inhibitors based on surfactants, such ammonium dodecyl sulfate (ADS), have also been investigated.

6.3.3.1 Benzotriazole

Thermodynamic analysis indicates that benzotriazole is an effective corrosion inhibitor for copper over a wide pH and potential range. This is shown graphically in the Pourbaix diagrams in Fig. 6.20; in this figure, the addition of BTAH induces a passive CuBTA region in addition to the passivation of copper by its own oxides, shown in Fig. 6.13a for comparison. The range of the passive CuBTA region expands as BTAH concentration is increased, up to a BTAH concentration of around 0.01 M, beyond which no further expansion is observed.

Surface characterization techniques such as surface-enhanced Raman spectroscopy have been used in conjunction with thermodynamic analysis to determine the

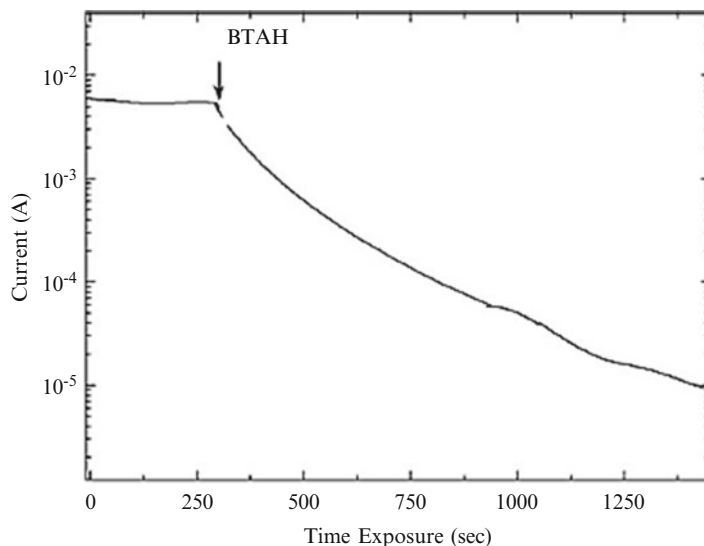
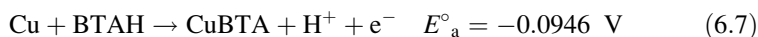
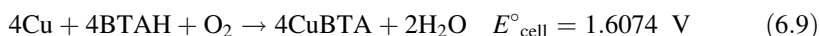


Fig. 6.21 Anodic current of copper over time at an applied potential of 0.1 V in a solution of 3 wt% nitric acid. At the point indicated, 0.02 M BTAH is added. As can be seen from the figure, the BTAH immediately but gradually reduced the transient current, indicating the slow formation of a passive film [30]

morphology of the CuBTA film. The film is thought to form initially by absorption of BTAH molecules on to the copper surface and then by reduction of oxygen:



This gives the overall reaction:



BTAH is the dominant species in solution at pH 2 and applied potential of -0.7 V. Under these conditions, surface-enhanced Raman spectroscopy has been used to show that the CuBTA film forms when the lone pair of the BTAH nitrogen atoms in the triazole ring bond to the copper surface. The adsorbed molecules are oriented perpendicularly to the copper surface and pack closely, forming a continuous adsorbed film.

Although thermodynamically and sterically favorable, BTAH has relatively slow reaction kinetics which may limit its suitability for CMP. In the presence of chloride ions, CuBTA films form rapidly. However, chloride ions can cause pitting of the copper surface, so great pains are taken to ensure that they are eliminated from CMP process streams, slowing the BTAH reaction kinetics. In a study, shown in Fig. 6.21, the anodic current generated by copper in nitric acid free of chloride ions was recorded

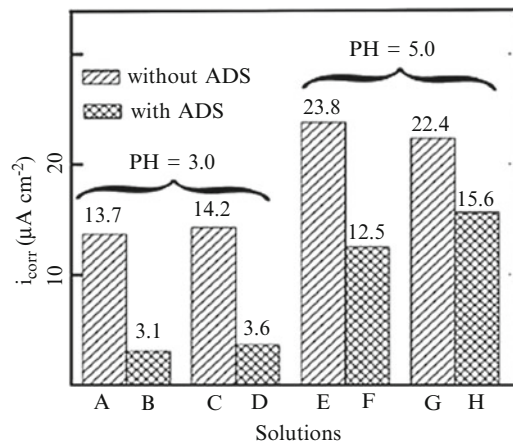


Fig. 6.22 Corrosion currents for copper rotating disc electrodes in various solutions containing 0.13 M of acetic acid. Solutions A, B, C, and D are at pH = 3 while E, F, G, and H are at pH = 5. Additionally, solutions A, B, E, and F contain 1 wt% H_2O_2 while the remaining solutions (C, D, G, and H) contain 5 wt% H_2O_2 . ADS is added to one of each type of solution and substantially decreases the corrosion current in all cases [36]

while BTAH was added to the solution. While a passive film did form, as indicated by the reduction in anodic current, the process occurred slowly and several minutes elapsed before the anodic current dropped by an order of magnitude. Despite these kinetic concerns, the ready availability of and body of knowledge surrounding BTAH mean that it is still the most widely used corrosion inhibitor in Cu CMP.

6.3.3.2 Surfactants as Corrosion Inhibitors

Due to these kinetic concerns, and concerns regarding its environmental impacts, a number of surfactants have been investigated as alternatives to BTAH. Surfactants are able to interact with the copper surface, allowing these chemicals to also behave as corrosion inhibitors in CMP. One such substance, ADS, is shown in experiments with rotating disc electrodes over a range of acidic pH values to reduce the corrosion current by a factor of 2 or more. These results, shown in Fig. 6.22, indicate that surface passivation is enhanced when ADS is present in solution.

The rate at which passivation occurs is also important in determining if a surfactant is effective as a CuCMP slurry additive. Two studies with ADS used in conjunction with low concentrations of BTAH suggest that ADS does in fact have faster reaction kinetics than BTAH in isolation. In one study [37], the anodic current of copper in solutions of hydrogen peroxide, 3 mM ADS, and varying concentrations of BTAH (shown in Fig. 6.23) is recorded over a period of 5 min. The results indicate that both BTAH and ADS effectively passivate the copper surface. However, the onset of passivation is slightly more rapid for ADS, with or without BTAH, and

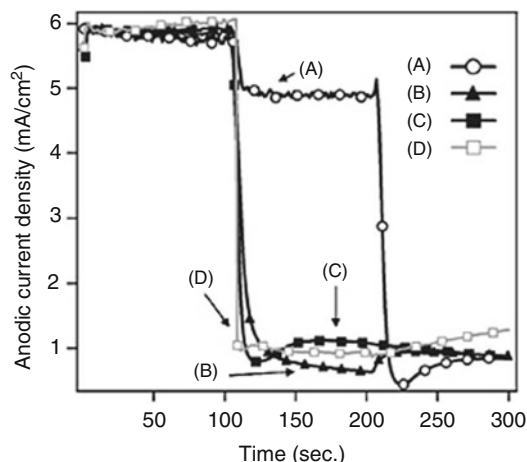


Fig. 6.23 The anodic current density transient for copper in solutions with 1 wt% glycine, 5 wt% H_2O_2 , pH = 4, and varying amounts of BTAH and ADS. Solution A contains 0.5 mM of BTAH and 3 mM of ADS, added at 100 and 200 s, respectively. Solution B contains the same concentrations of the inhibitors, added in reverse order. Solution C also contains the same inhibitor concentrations, both added at 100 s. Solution D contains 10 mM of BTAH added at 100 s, followed by 3 mM of ADS added at 200 s [37]

the degree of passivation is greater. The proposed mechanism for these varying passivation rates is that ADS hemi-micelles adhere strongly to the copper surface, preventing further reaction, while BTAH adsorbs between the ADS hemi-micelles. According to this model, ADS and BTAH are in competition for adsorption sites; this is supported by the results shown in Fig. 6.23, where a slight increase in anodic current is observed when either ADS or BTAH is added to a solution already containing the other chemical, regardless of the order in which they are added.

In a second study [38], in situ measurements of the open circuit potential (OCP) were made while a copper electrode was polished, held stationary, and then polished again in a slurry containing ADS and other chemicals. The results, shown in Fig. 6.24, show that the OCP increases by 50 % or more while the electrode is held stationary compared to during polishing. This supports the model of Cu CMP as a process of passivation, film removal, and re-passivation. As in the first study described here, the rate of passivation is greater for solutions containing ADS than for BTAH (Fig. 6.24, curves e and f).

The quality of the copper surface produced after polishing with ADS has been assessed by atomic force microscopy such as those shown in Fig. 6.25. In this example, the copper surface was polished in a slurry containing ADS as well as hydrogen peroxide, glycine, and silica particles. The resulting surface roughness is very low, with a root-mean-square surface roughness (R_a) of 5.1 Å.

A number of other surfactant-type corrosion inhibitors, including Triton X-100 and dodecyl trimethyl ammonium bromide (D-TAB), have been characterized for use in CMP. The outcomes of these and similar studies can be found in the literature.

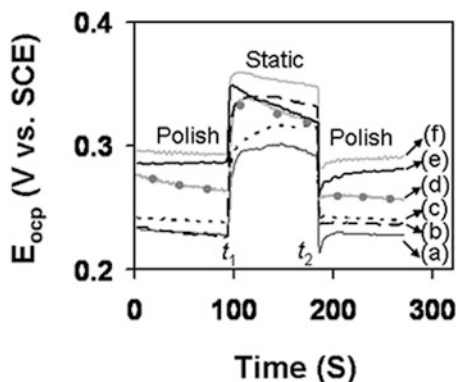


Fig. 6.24 Open circuit potentials for copper discs in polishing and static conditions. Polishing was carried out in a solution of 1 wt% glycine and 5 wt% H_2O_2 at $\text{pH} = 4$ (curve a) with additions of (b) 1 mM BTAH, (c) 1 mM BTAH + 1 mM ADS, (d) 10 mM BTAH, (e) 1 mM ADS, and (f) 10 mM ADS [38]

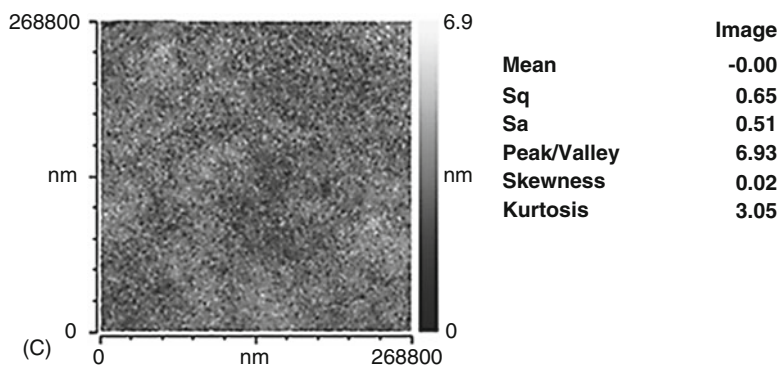


Fig. 6.25 Copper surface after polishing in a slurry containing 0.4 mM of ADS, 3 wt% fumed silica particles, 1 wt% glycine and 5 wt% H_2O_2 at $\text{pH} 4$ [38]

6.3.4 Efficacy of Evaluating Copper CMP Through Electrochemical Techniques

Significant progress has been made in identifying and testing of chemical solutions suitable for CMP. The progression from nitric acid to ammonium hydroxide to hydrogen peroxide has been shown to have a strong electrochemical justification, both theoretical and experimental, and has resulted in improved polishing outcomes for copper. Polish quality has been further enhanced by the use of the corrosion inhibitors benzotriazole and ADS. The suitability of these additives also has a firm basis in electrochemical theory and has moreover been demonstrated experimentally.

Table 6.1 Data for several buffer systems

Buffering agent	pK_a	Useful pH range
Citric acid	3.06	2.1–7.4
	5.75	3.0–6.2
Acetic acid	4.74	3.8–5.8
Ammonia	9.26	8.2–10.2
Phosphate	2.12	1.1–3.1
	7.21	6.2–8.2
	12.32	11.3–13.3

However, CMP is a complex process. As well as the electrochemical considerations discussed here, the success or otherwise of the technique depends on the chemical interaction with the abrasive particles and the pressure and velocity of polishing. Although some workers have attempted to electrochemically characterize various chemistries in polishing-like conditions, the full effects of slurry transport to and from copper surface has not been examined and remains a key unanswered question in understanding copper CMP.

6.3.5 Buffers in CMP slurries

Control of slurry pH is important for CMP process stability since pH affects removal rate and the formation of defects. The pH of slurries can drift globally or locally due to exposure to air or a redox reaction that occurs during metal CMP, for example. High pH slurries absorb CO_2 from the air forming carbonic acid which lowers the pH over time. Reactions of metals with slurries can locally generate H^+ or OH^- ions that will locally lower or raise the pH, respectively.

The variation of pH can be controlled by adding buffers to the slurry system. For acidic slurries, an acid buffer is required which is a mixture of a weak acid and its salt, which is formed by the reaction of the weak acid with a strong base. A good example of this is the citric acid buffer system, citric acid and potassium citrate. Potassium citrate is formed from the reaction of citric acid and potassium hydroxide. Basic slurries need a basic buffer system, a mixture of a weak base and its salt which is formed by the reaction of a weak base and a strong acid. An example of a basic buffer is ammonium hydroxide and ammonium chloride. Ammonium chloride is formed by the reaction of ammonium hydroxide with hydrochloric acid. Values for pK_a (negative logarithm of the dissociation constant) and pH range for several buffer systems are shown in Table 6.1. Note that the useful pH is typically close to pK_a .

6.3.6 Polishing of Highly Doped Silicon

In this chapter the reaction of metals with solutions has been discussed. Semiconductors such as silicon and germanium are another group of materials that can display

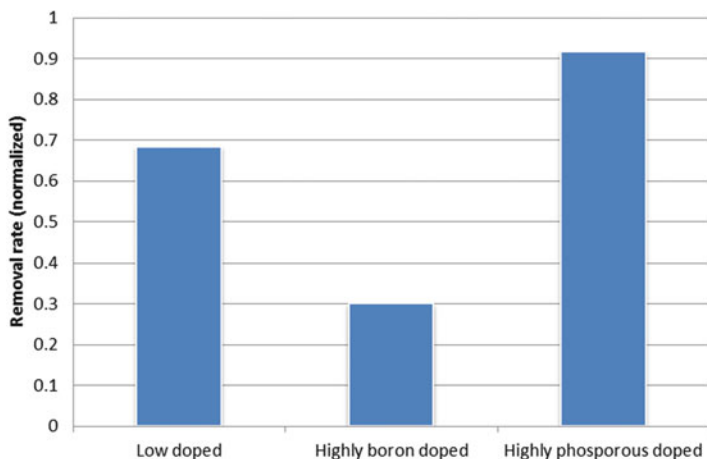


Fig. 6.26 Effect of doping on polish rate of polysilicon, after 20 min of polish (3 psi pressure and 40 rpm in a colloidal slurry at pH = 10.4) [40]

metallic like behavior and which are used in integrated circuit manufacturing. Integration schemes for these materials often require them to be removed by CMP. It has been shown that doping of semiconductors affects the CMP polish rate [39–43].

Polycrystalline silicon (polysilicon) is an important semiconductor which is used for filling vias and making interconnections in integrated circuits. Doping polysilicon with phosphorous increases the CMP removal rate while boron doping decreases the removal rate as shown in Fig. 6.26. This effect is not fully understood. One model postulates that dopant atoms compete with silicon in reacting with the slurry [40, 41]. However, the dopant concentration is significantly less than the silicon concentration ($\ll 1$ at.%) and it is unlikely that a competitive reaction could explain the polish rate changes. Another hypothesis is that the difference between the silicon and the dopant atom size generates stress in the material, thereby influencing the polish rate [41, 42]. This is also unlikely since various experiments have shown that the polish rate is more dependent on the charge of dopant than the size. The third model, shown schematically in Fig. 6.27, relates the removal rate change to the influence of the electric field formed by dopants. It has been shown that weakening the Si–Si bonds increases the polysilicon polish rate. Strong polarizers such as hydroxyl anions at high pH weaken Si–Si bonds and can increase the removal rate [41]. Impeding or assisting the transportation of hydroxyl anions on the polysilicon surface directly affects the polish rate. On the other hand, dopants form a depleted layer on the wafer surface, B⁻ ions repelling OH⁻ while the P⁺ ions attract OH⁻ to the silicon surface and thereby influence the OH⁻ transportation at the surface [41, 43].

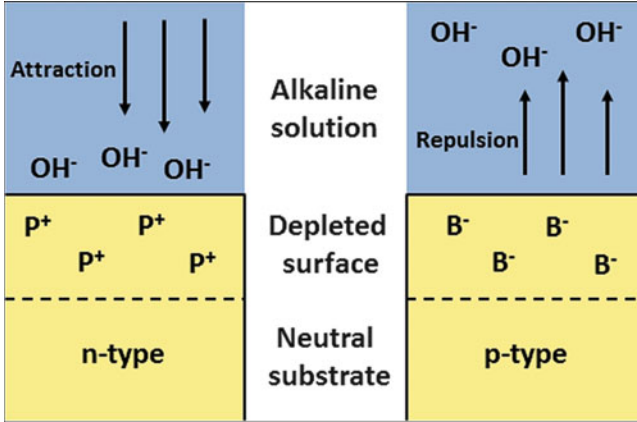


Fig. 6.27 Schematic illustration of the model which describes the electric effect of dopants on polysilicon polish [41]

6.4 Emerging Applications: CMP of Noble Metals

Unique features of CMP make it popular in many areas where smoothness and high surface quality are required. Polishing of noble materials such as platinum, ruthenium, and iridium is another important application of CMP. These materials are widely used in electrical industry because of their high work function, conductivity, and chemical stability. For example, iridium and platinum are known as noticeable candidates for gate electrodes of p-channel devices and as bottom electrodes for capacitors [44–47]. The application and effect of CMP on these noble materials are briefly explained below.

6.4.1 Platinum and Iridium

High work function of materials such as platinum and iridium makes them useful as diffusion barrier capacitors for gate electrodes and molecular device substrates [45, 48]. However, there are many issues in polishing these noble materials. The main problem relates to their inert properties. Platinum is a strong corrosion-resistant material and therefore it shows polish rates below 10 nm/min. Iridium is also difficult to react and is almost inert to all acids and even strong oxidizers at room temperature. There are other problems such as the hardness of iridium which make the abrasive choices limited. The polish rate of iridium is less than 50 nm/min and takes long time to planarize the surface. There have been studies working on increasing the polish rate by using slurries containing abrasives like alumina or iridium oxide and chemicals such as high PH solutions and oxidizer additives [45, 49, 50]. Because of the low polish rate and difficulty in patterning these noble materials, more study is required to commercialize the role of platinum and iridium.

6.4.2 Ruthenium

Ruthenium is a popular noble bottom electrode. This material shows low current leakage and compatibility to high dielectric materials. Like other noble materials, CMP of ruthenium is difficult due to the high hardness and corrosion resistance. Oxide formation can improve the polish rate because it is soluble in aqueous solutions. An example of slurry for ruthenium polishing is highly acidic ceric ammonium nitrate which acts as a strong oxidizer to ruthenium and helps to increase the polish rate. However, the low PH environment is not preferred for polishing due to corrosion and this solution is not popular for ruthenium polishing [47, 48]. It has been shown that alumina or silica abrasive in solutions such as NIO_4 and KIO_4 is another interesting candidate for ruthenium polishing. Maximum polish rate was achieved at PH ~ 6 and was lower than 100 nm/min [46, 48, 51, 52].

6.5 Electrochemically Induced Defects in CMP

The mechanism of metallic contamination can be classified into two types: electrochemical and surface chemical [53]. This is based on electrons being transferred, whether there exist oxidation/reduction reactions and the possibility of valence changes of the elements during the contamination process. In this section we will only concentrate on the electrochemically induced defects.

Cu CMP is a typical example of metal that is susceptible to electrochemical defects. Cu is not chemically stable and it is not self-passivated (that is, it doesn't grow a protective layer) which signifies that Cu will interact with other chemical reagents during the wet CMP process and becomes susceptible to chemically induced defects [54]. The chemically induced defects in Cu CMP are derived from classical corrosion processes. They can be characterized into three types [55]: pitting corrosion, galvanic corrosion, and chemical etching which are discussed in the following sections.

6.5.1 Galvanic Corrosion and Photo-Induced Defects

The Cu dual damascene process, shown in Fig. 6.9, is used in the fabrication of copper interconnect structures, in which chemical mechanical polish, CMP, is used to planarize and remove electroplated copper overburden [56–60]. Prior to the electrodeposition of Cu, a thin diffusion barrier layer material typically Ta and/or TaN and a Cu seed layer are deposited onto the substrate, specifically into the trenches and vias created by reactive ion etching [56, 57]. In the final stage of Cu CMP, both Cu and the barrier layer (Ta and/or TaN) are subjected to CMP and are exposed to polishing slurries [56, 57]. Cu (more noble cathode) and the barrier metal (less noble anode) form a galvanic couple while immersed in the polishing

slurry and may induce preferential corrosion of either the barrier material or Cu by galvanic corrosion [56, 57, 59–61]. Shortly afterwards, “fangs” are usually observed at the Cu-barrier interface [59].

CMP slurry provides the conductive pathway between the more noble cathode and the less noble anode [59]. The most common oxidant in slurries used for copper CMP is hydrogen peroxide; however, it has a disadvantage that it decomposes easily decreasing its oxidizing strength [57]. Many studies have been carried out on the influence of slurry composition and pH on the nature and extent of such galvanic corrosion. Tamilmani et al. [57] in their study showed through electrochemical polarization measurements that galvanic corrosion between abraded Cu and Ta is a function of pH of the two slurry systems used (hydroxylamine and peroxide solutions) and was found to be the lowest at pH 4. Brusic et al. [58] in their study also used polarization curves to predict the likelihood of galvanic corrosion between Cu and Ta when immersed in an aqueous electrolyte at different pH values. Assiongbon et al. [59] investigated the extent of galvanic corrosion between Cu and Ta on a partially Cu-covered Ta disk by combined electrochemical impedance spectroscopy with potentiodynamic polarization and galvanic current measurements in two CMP slurry solutions.

During the CMP process, galvanic corrosion of metals is determined commonly by potentiodynamic polarization measurement where the anodic branch of the Ta polarization curve intersects the cathodic branch of Cu forming a galvanic couple [56–59]. In galvanic couples, the less noble metal forms the anode (typically Ta or TaN) and the other acts as the anode (Cu). Lin et al. [56] used potentiodynamic polarization curves of Cu and the barrier material TaN exposed to commercial slurries to show a galvanic couple when the anodic branch of TaN polarization curve intersects the cathodic branch of Cu in the slurries used. Also, it should be noted that the galvanic potential and the galvanic current density can be estimated from the point of intersection of the anodic portion of the TaN curve and the cathodic portion of the Cu portion.

In the estimation of the galvanic current, the anodic portion of the polarization curve represents the metal corrosion reaction while the cathodic portion represents the reduction reaction, which is responsible for metal corrosion due to its chemistry [56, 57]. When abrasion occurs during CMP, galvanic corrosion is increased during which the anodic reaction is the oxidation of the active metal (Ta) and the cathodic reaction is the reduction of the noble metal ions (Cu) in the solution [56, 57]. Tamilmani et al. [57] showed that Ta corrosion is enhanced when Ta and Cu form a couple and are abraded. Furthermore, it was proven that galvanic current density increased when subjected to abrasion in all chemistries. Galvanic current density during abrasion went as high as $500 \mu\text{A}/\text{cm}^2$ in hydroxylamine solutions and $120 \mu\text{A}/\text{cm}^2$ in hydrogen peroxide at pH 6 and 8, respectively [57].

Faradaic reactions are observed when measuring the corrosion currents [59]. After metallic CMP, the most likely area of the substrate that is exposed is the oxide layer. An oxide film is most likely to be formed on the polished Ta surface when the sample is introduced into an aqueous electrolyte [53]. The anodic

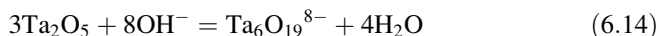
oxidation (corrosion) reaction of Ta surface partially covered in oxide occurs in the following three steps [59, 62]:



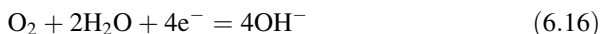
with the net reaction as follows [59, 63]:



Electro-dissolution of the Ta oxide occurs as follows [59, 62]:



when peroxide slurries are used, the OH^- ions present in reaction 14 are provided as a result of the electro-reduction (catalytic breakdown) of H_2O_2 [59]. The solution pH determines the intermediate steps of H_2O_2 reduction. In alkaline solutions, H_2O_2 reduces in the following two steps [59–61]:



with the net reaction written as [61]:



The intermediate reaction 16 involves the chemisorption of oxygen for the reduction of H_2O_2 . This takes us to the corresponding cathodic reaction that originates from hydrogen evolution or O_2 reduction [59]:



Reaction (6.18) is likely to occur in acidic media while reaction (6.16) is more dominant in a neutral or alkaline environment. In both cases, however, the alkalinity increases at the cathode.

Pertaining to the copper electrode (cathode), Cu dissolution/oxidation occurs in the following steps [59]:

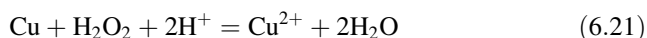
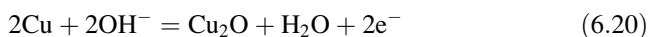
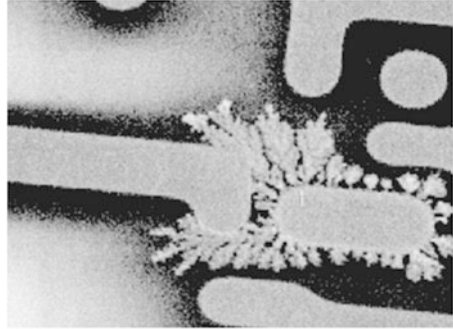
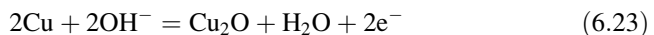
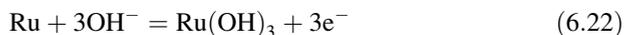


Fig. 6.28 Light-induced copper dendrite growth during post-CMP cleaning [55]



So far, we have concentrated on galvanic corrosion between Cu and the barrier metal Ta and its nitrides; however, the integration of Ru as a barrier material is being considered as an alternative material for Ta/TaN in the fabrication of Cu interconnect structures. The benefits of switching to Ru are its lower resistivity ($7 \mu\Omega \text{ cm}$) compared to Ta ($14 \mu\Omega \text{ cm}$) and TaN ($200 \mu\Omega \text{ cm}$) and Ru is more electrically conductive than Ta and its nitrides [60, 61]. Ru possesses advanced barrier characteristics such that it can support direct electro-deposition of Cu lines without using seed layers [60, 61]. However, due to the noble metal characteristics of Ru, it is difficult to integrate completely Ru barrier films in Cu interconnects due to the fact that Ru induces galvanic corrosion on the adjacent Cu lines during the CMP process of the multilayer components [60, 61]. Due to this, in the wet CMP environment, it is rather difficult to remove material in Ru-CMP without inducing surface defects as Ru forms a strong galvanic couple with Cu, and in this case, it is typically the Cu lines of the Ru-Cu structure that corrodes as a result of the coupling [60, 61]. In this galvanic coupling, Ru acts as the cathode while Cu acts as the anode.

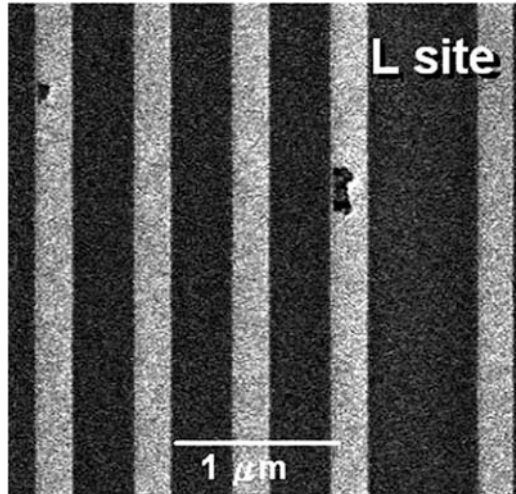
Many studies have been carried out on the control of this galvanic corrosion of Cu during CMP of Ru. It can be concluded that there exists a large difference between the OCPs (E_{oc}) of Ru and Cu exposed to reactive CMP slurry; this large difference of E_{oc} is the cause of the galvanic corrosion of Cu [60, 61]. The predominant oxidation anodic reactions for Ru and Cu are as seen below [60, 61]:



where both $\text{Ru}(\text{OH})_3$ and Cu_2O are passivating species at the anode. However reaction (6.22) is followed by a chemical conversion of $\text{Ru}(\text{OH})_3$, where Ru is converted to RuO_2 by H_2O_2 in the solution [58]. The cathodic branch is caused by reaction (6.18).

Photo-induced electron is another cause of galvanic corrosion [55]. Figure 6.28 shows a light-induced copper dendrite growth on the surface of a patterned wafer. This unique corrosion mechanism usually occurs during the post-CMP cleaning steps [55].

Fig. 6.29 SEM image of the via feature which has pits on the surface [64]



This occurs when the Cu is connected to $p-n$ junctions, and is exposed to light. Within this $p-n$ junction, there exist excited electron-hole pairs. The electrons are shifted toward the n -type material while the holes move toward the p -type material by existing electric fields. Copper connected to the p -type and n -type material forms the anode and cathode, respectively. The result is a depletion of copper from the anode (Cu is oxidized and the electrons are canceled by photo-induced holes) and an accumulation of Cu at the cathode (Cu is reduced by the photo-induced electrons) [55]. The dendrite defect can be controlled by avoiding incident illumination during post-CMP cleaning process.

6.5.2 Pitting

Pitting corrosion is a localized form of corrosion which forms small holes on the surface of metals. The higher corrosion rate increases the pitting on the surface and consequently the surface roughness. Figure 6.29 shows an example of pitting defect on the surface of copper interconnects. To control the pitting behavior the corrosion mechanism should be understood and the polish environment needs to be controlled carefully [65].

In copper the pitting occurs in both acidic and basic solutions with the presence of oxidizers. By using the Pourbaix diagram it can be realized that in acidic solutions the copper corrodes to Cu^{2+} and a cathodic reaction happens before the passive film forms to protect the surface. Defects such as scratches and grain boundaries, and impurities such as halides, SO_4^{2-} , PO_4^{3-} , NO_3^- , and HCO_3^- , act as copper pitting agents and help initiating localized galvanic corrosion on the surface. These anions specifically prevent any passive film formation by reacting

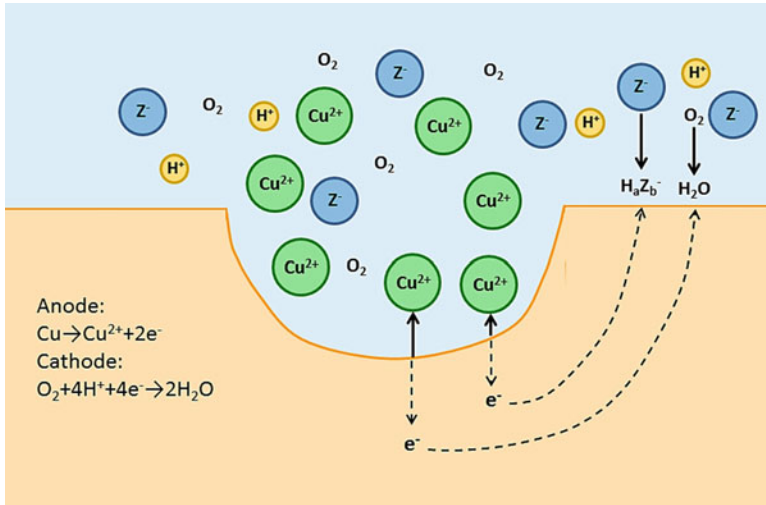


Fig. 6.30 The schematic mechanism of pitting corrosion on copper CMP in acid solution (6.4a). Z^- represents anion ions such as F^- and NO_3^-

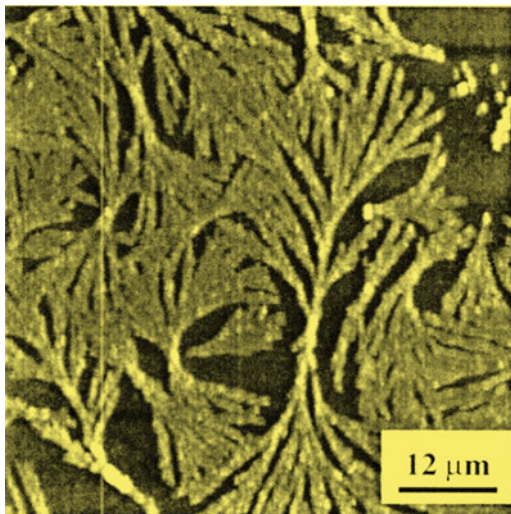
with the metastable Cu_2O and releasing Cu^{2+} ions into the solution. Figure 6.30 schematically illustrates the pitting behavior in acidic environment. In this process the potential gradient and the electromigration occur between the localized anodes which form inside and the cathodes which form outside the pit. In basic solutions, Cu_2O passive film formation hinders the corrosion and pitting occurs when the oxide is removed mechanically [65, 66].

Adding corrosion inhibitors and additives such as benzotriazole (BTAH) in the acidic regime can reduce the pitting effect on metals. This happens due to the formation of a nonnative protective film on the surface of metal. Another useful method to decrease the pitting effect is to use a cathodic protection such as tantalum or titanium [64, 65].

6.5.3 Redeposition of Material

As mentioned earlier, chemical mechanical polishing of materials—especially metals—is mainly based on the etching of the surface. Chemical reaction and etching of the surface lead to the release of anions into solution which can be redeposited again on the surface. This undesired phenomenon forms a rough surface with a dendritic texture. Copper polishing is an example of the redeposition as shown in Fig. 6.31. In this figure, the dendrite structure is formed due to the redeposition of $\text{Cu}(\text{OH})_2$ precipitation on the polished surfaces [67, 68]. Redeposition of silica abrasives is another unwanted post-CMP issues which can leave a rough surface

Fig. 6.31 AFM topography of redeposited copper salt dendrites [65]



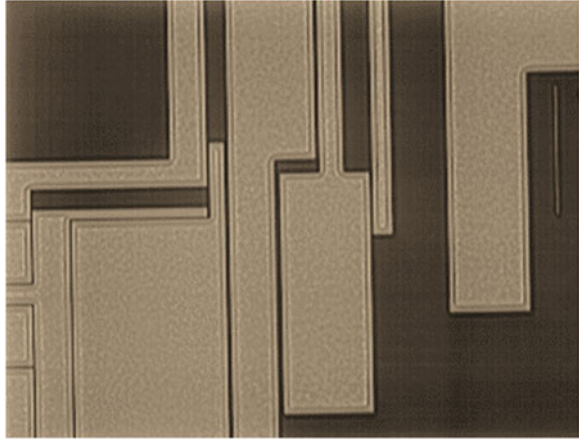
after polishing [69]. The redeposition of alumina abrasives after copper polishing is an example of the abrasive redeposition. There have been many cleaning studies aimed at preventing redeposition and it has been shown that the electrostatic repulsion of anions from the wafer surface can be a helpful cleaning method. If the polished surface and the anions carry the same charge repulsion occurs and if they have opposite charge attraction takes place [69, 70]. The repulsion and consequently the redeposition prevention occur by using the suitable chemical conditions such as changing the pH and solution zeta potential.

6.5.4 Etching and the Development of Texture

When two dissimilar metals are immersed in an electrolyte and are placed in contact, one metal will undergo oxidation and the other reduction, leading to etching of the first metal and redeposition of the second metal [55, 64]. Usually, etching solutions are made up of inhibitors and surface active compounds; due to this Cu etching is usually followed by deposition of corrosion products, Cu (I) compounds, on the surface [71].

During Cu CMP, the use of low pH slurries in the absence of corrosion inhibitors results in high static etch rates leading to enhanced surface texturing. This is shown in Fig. 6.32, where etching and surface texturing occurred in patterned wafers exposed to a Cu peroxide-based slurry and a static etch rate of 400 A/min [55, 64]. This type of texturing occurs in wide structures that are coated during copper electroplating in which the Cu at the middle of the structure is thinner than the Cu thickness at the edge. Since the center is thinner it is initially unpolished since the polishing pad is supported by the edges. The center undergoes chemical etching. Excess Cu loss

Fig. 6.32 Texturing defect induced by a high static etch slurry [64]



and surface roughening can occur if the unpolished center of advances below the ILD surface while there is Cu in the field regions [55, 64]. Cu^{2+} ions or a cupric complex is the most common etching reaction product of Cu CMP [64]. Cu^{2+} in the presence of complexing agents such as glycine enhances peroxide activity [72] contributing to increasing localized etching and texturing. However, an increasing peroxide concentration will lead to a decline in both the wet etch rate and polish rate of Cu which can be explained by the stability of the passivating layer [55]. Static etch rates can be controlled by increasing the pH of the slurry and implementing inhibitors like BTAH.

6.6 Conclusion and Future Directions

Chemical mechanical polishing is an essential enabling technology in modern semiconductor manufacturing. Electrochemical techniques have furthered the technology and are capable of characterizing the process with increasing accuracy. Topics of future research in CMP are closely related to the future direction of the semiconductor manufacturing industry as a whole. Some specific areas of progress are outlined below.

As described earlier in this chapter, galvanic interactions can influence the CMP process. As the range of metals involved in devices expands, the range of possible galvanic effects also expands. Using electrochemical research techniques can assist with assessing the effect of these interactions on CMP as part of the materials selection process.

Away from the semiconductor industry, CMP is also used to create atomically smooth surfaces for use (as an example) as substrates for molecular devices. While there is less commercial interest in such applications, CMP can be a significant

enabling technology in academic research. Academic users employ a very wide variety of materials, including noble metals such as platinum [73], to produce ultrasmooth substrates for biological devices; hard and brittle ceramics such as transparent neodymium-doped yttrium aluminum garnet (Nd:YAG), used in lasers [74]; and polymeric materials as substrates in MEMS and bio-MEMS devices [75]. CMP of these surfaces is often conducted by the researcher themselves on an ad hoc basis to enable their own research goals, leading to a strongly multidisciplinary body of research. This is a valuable resource for CMP researchers of all persuasions and a source of innovation in the field.

Critical dimensions for chip components are reducing to the extent that they are commensurate with the size of the defects generated by the CMP process. This trend is likely to continue in the future, according to Moore's Law [76]. Hence, the pressure to reduce defects is one of the primary drivers in CMP as it allows critical dimensions to continue to shrink.

Leading-edge silicon processing is carried out on 300 mm wafers. Within the next several years, 450 mm processing is expected to become the standard [77]. This is likely to greatly impact CMP as many polishing metrics, such as removal rate and fluid pressure, are radially dependent. Current research on scaling to 450 mm wafers is focused on slurry usage and dissipation of the frictional heat generated [78].

References

1. Beyer K (1999) IBM MicroNews 5:46
2. ITRS Roadmap: <http://www.itrs.net/Links/2012ITRS/Home2012.htm> Table FEP14
3. Tripathi A, Suni I I, Li Y, Doniat F, McAndrew J (2009) J Electrochem Soc 156:H555-H560
4. Plummer J D, Deal M D, Griffin P B (2000) Silicon VLSI Technology, Prentice Hall, Upper Saddle River, New Jersey
5. Lin F, Nolan L, Xu Z, Cadien K (2012) J Electrochem Soc 159:H482-H489
6. Lu Z, Lee S-H, Gorantla V R K, Babu S V, Matijevic E (2003) Mater Res 18:2323-2330
7. Bielmann M, Mahajan U, Singh R K (1999) Electrochem Sol-Stat Lett 2:401-403
8. Luo J, Dornfeld D A (2003) IEEE Trans Semi Manuf 16:469
9. Nolan L, Cadien K (2103) Wear 307:155
10. Steigerwald J M, Murarka S P, Gutmann R J (2004) Chemical Mechanical Planarization of Microelectronic Materials. Wiley-VCH, Weinheim, Germany
11. Bastaninejad M, Ahmadi G (2005) J Electrochem Soc 152:G720
12. Greenwood J (1984) In: Proceedings of the Royal Society of London. Series A, Mathematical and Physical Sciences 393:133-157
13. Philipossian A, Mitchell E (2003) J App Phys 42:7259-7264
14. Coppeta J, Rogers C, Racz L, Philipossian A, Kaufman F (2000) J Electrochem Soc 147 (5):1903-1909
15. Preston F. W (1927) J Society of Glass Technology XI :214-256
16. Luo Q, Ramarajan S., Babu S. V (1998) Thin Solid Films 335:160-167
17. DeNardis D, Rosales-Yeomans D, Borucki L, Philipossian A (2010) Thin Solid Films 518:3910-3916
18. Lee S-Y, Lee S-H, Park J-G (2003) J Electrochem Soc 150:G327-G332
19. Mazaheri A, Ahmadi G (2003) J Electrochem Soc 150: G233-G239

20. Li J, Lu X, He Y, Luo J (2011) *J Electrochem Soc* 158: H197-H202
21. Rogers C, Coppeta J, Racz L, Philipossian A, Kaufman, F.B, Bramono D (1998) *J Electronic Materials* 27:1082-1087
22. Seok J, Sukam C, Kim A, Tichy J, Cale T (2003) *Wear* 254 :307–320
23. Lu Y. S, Li N, Wang J, Zhang T, Duan M, Xing X.L (2011) *Adv Mat Res* 215:217-222
24. Wijekoon K, Lin R, Fishkin B, Yang S, Redeker F, Amico G, Nanjangud S (1998) *Solid State Technology* 41(4)
25. Cook LM (1990) *J. Non-Crystalline Solids* 120:152-171
26. Ziomek-Moroza M, Miller A, Hawk J, Cadien K, Li D.Y (2003) *Wear* 255:869-874
27. Lim G, Lee J-H, Son J-W, Lee H-W, Kim J (2006) *J Electrochem Soc* 153:B169-B172
28. Hernandez J, Wrschka P, Oehrlein GS (2001) *J Electrochem Soc* 148:G389-G397
29. Aksu, S (2005) *Mater Res Soc Symp Proc* 867:W1.6.1 - W1.6.6
30. Carpio R, Farkas J, Jairath R (1995) *Thin Solid Films* 266:238-44
31. Ein-Eli Y, Abelev E, Rabkin E, Starosvetsky D (2003) *J Electrochem Soc* 150:C646-C652
32. Ein-Eli Y, Abelev E, Starosvetsky D (2004) *J Electrochem Soc* 151:G236-G240
33. Aiken JK, Howard DK, Popplewell AF (1965) Inhibiting Copper Corrosion. British Patent 994,409
34. Tromans D (1998), *J Electrochem Soc* 145: L42-L45
35. Cadien KC, Nolan L (2012) *Handbook of Thin Film Deposition*. Seshan, K (Ed.), Elsevier, Amsterdam
36. Zheng JP, Roy D (2009) *Thin Solid Films* 517:4587-4592
37. Hong Y, Devarapalli VK, Roy D, Babu SV (2007) *J Electrochem Soc* 154:H444-H453
38. Hong Y, Patri UB, Ramakrishnan S, Roy D, Babu SV (2005) *J Mat Res* 20:3413-3424
39. Yang W L, Cheng C, Tsai M, Liu D, Shieh M (2000) *IEEE Elect Dev Lett* 21: 218–220 doi:[10.1109/55.841301](https://doi.org/10.1109/55.841301)
40. Forsberg M, Keskitalo N, Olsson J (2002) *Microelectronic Engineering* 60:149–155. doi:[10.1016/S0167-9317\(01\)00591-3](https://doi.org/10.1016/S0167-9317(01)00591-3)
41. Liu D-G, Tsai M S, Yang WL, Cheng C-Y (2001) *J Electronic Materials* 30:53–58. doi:[10.1007/s11664-001-0214-9](https://doi.org/10.1007/s11664-001-0214-9)
42. Senna JR, Smith RL (1995). Paper presented at the 8th Int Conf on Solid State Sensors and Actuators, and Eurosensors IX, Stockholm, Sweden, 25-29 June 1995.
43. Watanabe J, Yu G, Eryu O, Koshiyama I, Izumi K, Nakashima K, Kodama K (2005) *Precision Engineering* 29(2):151–156. doi:[10.1016/j.precisioneng.2004.06.006](https://doi.org/10.1016/j.precisioneng.2004.06.006)
44. Evans D (2002). The Future of CMP. In: *MRS Bulletin*. <http://www.mrs.org/publications/bulletin>
45. Kim I-K, Cho B-G, Park J-G, Park J-Y, Park H-S (2009) *J Electrochem Soc* 156:H188 doi:[10.1149/1.3058594](https://doi.org/10.1149/1.3058594)
46. Lee W, Park H, Lee S, Sohn H (2004) *Applied Electrochem* 34:119–125
47. Peethala BC, Babu SV (2011) *J Electrochem Soc* 158:H271. doi:[10.1149/1.3528942](https://doi.org/10.1149/1.3528942)
48. Lee S-H, Kang Y-J, Park J-G, Lee S-I, Lee W-J Chemical Mechanical Planarization of Ruthenium for Capacitor Bottom Electrode in DRAM Technology. <http://www.electrochem.org/dl/ma/203/pdfs/0446.pdf>
49. Mainka G, Beitel G, Schnabel RF, Saenger A, Dehm C (2001) *J Electrochem Soc* 148:G552. doi:[10.1149/1.1396339](https://doi.org/10.1149/1.1396339)
50. Kim N-H, Ko P-J, Kang S K, Lee W-S (2007) *Microelectronic Engineering* 84:2702–2706. doi:[10.1016/j.mee.2007.05.027](https://doi.org/10.1016/j.mee.2007.05.027)
51. Kim I-K, Kang Y-J, Kwon T-Y, Cho B-G, Park J-G, Park J-Y, Park H-S (2008) *Electrochem and Solid-State Letters* 11: H150. doi:[10.1149/1.2901544](https://doi.org/10.1149/1.2901544)
52. Cui H, Park J-H, Park J-G (2012) *J Electrochem Soc* 159:H335–H341 doi:[10.1149/2.103203jes](https://doi.org/10.1149/2.103203jes)
53. Zhang LM, Raghavan S, Weling M (1999) *J Vac Sci Technol B* 17:2248-55
54. Choiu WC, Chen YC, Lee SN, Jeng SM, Jang SM, Liang MS (2004) *IEEE* 8:127–129

55. Miller AE, Feller AD, Andryushchenko TN, Cadien KC (2003) ASM Handbook. vol 13A ASM International, p 164–9
56. Lin JY, Wang YY, Wan CC, Feng HP, Cheng MY (2007) *Electrochem Solid-State Lett* 10: H23-H6
57. Tamilmani S, Huang W, Raghavan S (2006) *J Electrochem Soc* 153:53-9
58. Brusich V, Kistler R, Wang SM, Hawkins J, Schmidt C (1998) *Elec Soc S* 98:119-25
59. Assiongbon KA, Emery SB, Gorantla VRK, Babu SV, Roy D (2006) *Corrosion Science* 48:372-88
60. Peethala BC, Roy D, Babu SV (2011) *Electrochem and Solid-State Lett* 14:306-10
61. Turk MC, Rock SE, Amanapu HP, Teugels LG, Roy D (2013) *J Sol Stat Sci and Technol* 2: P205-P13
62. Assiongbon KA, Emery SB, Pettit CM, Babu SV, Roy D (2004) *Mater. Chem. Phys.* 86:347
63. Kerrec O, Devilliers D, Grout H, Chemla M (1995) *Electrochim. Acta* 40:719
64. Miller AE, Fischer PB, Feller AD, Cadien KC (2001) Chemically induced defects during copper polish. In: *Proceedings of the IEEE 2001 International Interconnect Technology Conference*, Piscataway, NJ, USA, 4-6 June 2001
65. Tsai T-H, Yen S-C (2003) *Appl Surf Sci* 210:190–205. doi:10.1016/S0169-4332(02)01224-2
66. Bentz DN, Jackson KA (2002) *Mat Res Soc Symp Proc* 697:1–6
67. Xu G, Liang H, Zhao J, Li Y (2004) *J Electrochem Soc* 151:G688. doi:10.1149/1.1787497
68. Vogt MR, Polewska W, Magnussen OM, Behm RJ (1997) *J Electrochem Soc* 144:L113-L6
69. Fyen W, Vos R, Teerlinck I, Lagrange S, Lauerhaas J, Meuris M, Mertens P, Heyns M (2000) The Ninth International Symposium on Semiconductor Manufacturing (P-55):415–418
70. Xu K, Vos R, Vereecke G, Doumen G, Fyen W, Mertens P W, Kovacs F (2005) *J Vac Sci & Technol B*: 23:2160. doi:10.1116/1.2052713
71. Ein-Eli Y, Starosvetsky D (2007) *Electrochimica Acta* 52:1825–1838
72. Hariharaputhiran M, Zhang J, Ramarajan S, Keleher JJ, Li Y, Babu SV (2000) *J Electrochem. Soc* 147:3820–3826
73. Islam MS, Jung GY, Ha T, Stewart DR, Chen Y, Wang SY, Williams RS (2005) *Appl Phys* 80:1385-1389
74. Li J, Zhu Y, Chen TC (2008) *Key Engineering Materials* 278:375-376
75. Zhong ZW, Wang ZF, Zirajutheen BMP, Tan YS, Tan YH (2005) CMP of PC, PMMA and SU-8 Polymers. Paper presented at Polytronic 2005. 5th International Conference on Polymers and Adhesives in Microelectronics and Photonics, pp.58-62, 23-26 Oct 2005
76. Nigam T, Yiang K-Y, Marathe A (2013) *Microelectronics to Nanoelectronics; Devices & Manufacturability*. In: Kaul, Anupama (Ed.), CRC Press, Boca Raton, USA
77. Davis J (2013) 450 mm – It’s bigger than you think. In: *Solid State Technology*. Available via DIALOG. http://www.electroiq.com/articles/sst/2013/06/450mm-_-it_s-bigger-than-you-think.html
78. Borucki L, Philipossian A, Goldstein M (2009) *Solid State Technology*, pp 10-13